A mechanistic study of nitrous oxide adsorption and decomposition on zirconia

T.M. Miller and V.H. Grassian *

Department of Chemistry, University of Iowa, Iowa City, IA 52242, USA
E-mail: vicki-grassian@uiowa.edu

Received 4 April 1997; accepted 17 April 1997

FT-IR spectroscopy and mass spectrometry have been used to study the adsorption and decomposition of nitrous oxide on zirconia. It was determined that zirconia cations in the 4+ oxidation state are the site for molecular adsorption of N_2O, whereas Zr^{3+} sites are active toward dissociative adsorption of N_2O at temperatures as low as 25°C. Catalytic decomposition of N_2O on ZrO_2 occurs at temperatures above 350°C and follows first-order reaction kinetics. Experiments utilizing isotopic labeling in conjunction with mass spectrometry were done to elucidate the details of the reaction mechanism. Based on the results presented here, a mechanism for N_2O decomposition on ZrO_2 is proposed.

Keywords: nitrous oxide decomposition, zirconia catalyst, FT-IR spectroscopy, mass spectrometry, lattice oxygen

1. Introduction

Nitrous oxide is an environmentally unacceptable molecule due to its atmospheric lifetime of more than 100 years and its contribution to processes harmful to the environment [1]. These processes include greenhouse warming, the depletion of ozone in the stratosphere, and the formation of acid rain. Nitrous oxide is an undesirable by-product from the industrial synthesis of adipic acid; it is formed in the last step of the synthesis when a cyclohexanone/cyclohexanol mixture is reacted with nitric acid to yield adipic acid. Recently, it has been suggested that N_2O emissions from the adipic acid industry account for 5–8% of anthropogenic sources of N_2O in the atmosphere [1]. Therefore, there is a great deal of interest in finding ways of reducing nitrous oxide emission. Several methods for reducing N_2O emission from adipic acid production have been proposed [2]. They include: (i) thermal decomposition of N_2O at high temperatures to produce N_2 and O_2, (ii) methane oxidation to produce CO_2, H_2O and N_2, (iii) catalytic decomposition and (iv) conversion of N_2O to nitric acid which can then be recycled back to the nitric acid feed.

Currently, ZrO_2 is the leading catalyst for commercialization of nitrous oxide abatement as zirconia and zirconia-based catalysts have recently been shown to be effective environmental catalysts for the decomposition of nitrous oxide [3–5]. In a previous study, we had investigated the interaction between nitrous oxide and zirconia [3]. It was determined that zirconia catalyzes the decomposition of nitrous oxide at temperatures above 350°C. It was postulated that zirconium cations were most likely involved in the decomposition reaction. However, the mechanistic details, in particular the role of defect sites and lattice oxygen atoms in the decomposition reaction, were not determined.

In general, it is known that defect sites, the most common being oxygen vacancies, are important in the surface chemistry and catalysis of metal oxides [7,8]. The electronic structure of the metal cation at these sites is significantly altered. Defect sites may be induced during the pretreatment of metal oxides. For example, heating ZrO_2 in vacuum results in an oxygen-deficient surface. Infrared spectroscopy and electron paramagnetic resonance of ZrO_2 samples have shown that the electronic structure at defect sites is consistent with Zr cations in the 3+ oxidation state [9].

It is also known that lattice oxygen atoms are often involved in reactions over high surface area metal oxides. Indeed for most selective oxidation catalysts, lattice oxygen atoms are incorporated into product molecules, to be replenished in a later step through the dissociative adsorption of molecular oxygen on the catalyst [10,11]. Therefore, much research has been done on the role of lattice oxygen in heterogeneous catalytic reactions [10–15]. The importance of lattice oxygen in other reactions involving high surface area metal oxides makes it reasonable to hypothesize that lattice oxygen atoms may be involved in the catalytic decomposition of N_2O to produce gas-phase molecular oxygen.

In this study, FT-IR spectroscopy is used to investigate the adsorption and decomposition of nitrous oxide on zirconia. Mass spectrometry in conjunction with isotopic labeling is used to further elucidate the details of the decomposition reaction.

* To whom correspondence should be addressed.

2. Experimental

An IR cell similar to the design of Yates and co-workers was used in the experiments described here [16]. The cell consists of a stainless-steel cube with two differentially pumped KBr windows and a sample holder. The sample holder consists of a stainless-steel grid held in place by a set of Ni jaws. The Ni jaws were mounted onto Ni power feedthroughs for sample heating. The temperature of the sample was monitored by spot-welding thermocouple wires to the center of the sample grid.

The sample was prepared by pressing zirconia powder onto a grid. For the IR studies, the zirconia was pressed into half of a stainless-steel grid, leaving the other side blank so that gas-phase measurements could be made. Approximately 13 mg of zirconia were pressed into a 3×1 cm^2 area of the grid. For the mass spectral studies, the zirconia was pressed into half of a gold-covered tungsten grid. Approximately 23 mg of zirconia were pressed into a 3×3 cm^2 area of the grid. Experiments without ZrO_2 present were done on both the stainless-steel grids and the gold-covered tungsten grids. N_2O did not decompose on the blank grids at the reaction temperatures used in this study.

The pressed ZrO_2 samples were calcined in air overnight at a temperature of 400°C prior to being placed in the stainless-steel cube. Once inside the cell, the sample was activated by heating to the desired activation temperature under vacuum for 30 min. In this paper, the activation temperature in degrees Celsius is given in parentheses, e.g. a sample heated to 500°C for 30 min is denoted as ZrO_2(500).

For the IR experiments, the IR cell was mounted on a linear translator inside of the FT-IR spectrometer so that both halves of the sample can be measured by simply moving the cell into the IR beam path. Infrared spectra were recorded with a Mattson RS-1000 equipped with a narrowband MCT detector. Typically, 250 scans were collected with an instrument resolution of 4 cm^{-1}. Background scans were collected by recording a spectrum of both the zirconia and blank sides of the grid before and after introduction of nitrous oxide into the IR cell.

Mass spectral data were collected with a UTI-Detector II quadrupole spectrometer (QMS). A leak valve connecting the stainless-steel cube to the mass spectrometer chamber was opened to maintain a pressure of 3.0×10^{-7} Torr into the mass spectrometer chamber for residual gas analysis (RGA).

High surface area zirconia (78 m^2/g) was purchased from Nanotek. The average diameter of the ZrO_2 nanoparticles is 14 nm. The zirconia samples consist of two crystallographic phases, the monoclinic and tetragonal, in approximately equal amounts. Ultrahigh purity nitrous oxide (99.99%) and CO (99.5%) were purchased from Matheson Gas Products. $^{15}N_2O$ was purchased from Isotec with a ^{15}N atom purity of 99.3%. $C^{18}O_2$ was also purchased from Isotec with an ^{18}O atom purity of 96.5%. All gases were used without further purification.

3. Results

3.1. ZrO_2 surface characterization as a function of activation temperature

Changes in the zirconia surface as a function of activation temperature in the 500–700°C temperature range were examined. An upper temperature limit of 700°C was used because heating the catalyst to temperatures above 700°C results in a significant decrease in surface area [17]. Figure 1 shows the IR spectra recorded from 3450 to 4000 cm^{-1} of the ZrO_2 catalyst held at room temperature after being heated to various activation temperatures between 500 and 700°C. The bands in this region can be assigned to terminal (t) and bridging (b) hydroxyl groups on the surface of the two zirconia phases – tetragonal (t) and monoclinic (m) [3]. The set of bands between 3700 and 3800 cm^{-1} are assigned to terminal OH groups, Zr–OH, and the set of bands between 3600 and 3700 cm^{-1} are assigned to bridging OH groups, Zr_n–OH ($n > 1$). As can be seen in figure 1, as the activation temperature increases, there is a decrease in the integrated areas of the bands due to hydroxyl groups on the surface. The decrease in hydroxyl group coverage is estimated from the integrated area of the entire O–H region

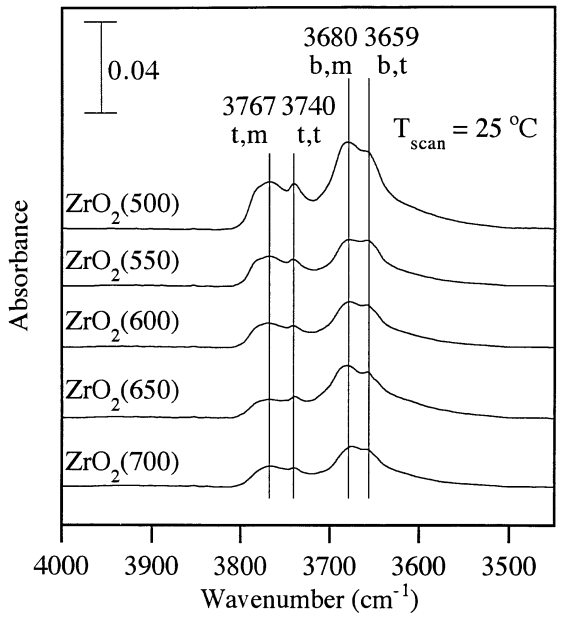

Figure 1. Transmission infrared spectra recorded from 3500 to 4000 cm^{-1} of ZrO_2 as a function of catalyst activation temperature from 500 to 700°C. The absorption bands in the spectra are assigned to terminal (t) and bridging (b) OH groups on the monoclinic (m) and tetragonal (t) phases. The bands are labeled as (site, phase), so for example (t, m) corresponds to a terminal OH group on the surface of the monoclinic phase.

to be approximately 50% for an activation temperature of 700°C compared to activation of 500°C.

As the surface is dehydroxylated, there is loss of oxygen from the sample and the metal oxide becomes reduced. In order to determine more about the electronic structure of the Zr cations, CO adsorption in conjunction with IR spectroscopy was used to probe the oxidation state of the Zr surface atoms. It has been previously shown that the IR absorption frequency for adsorbed CO differs by approximately 70 cm^{-1} for CO adsorbed on Zr^{4+} sites compared to CO adsorbed on oxygen-deficient sites identified by EPR spectroscopy as Zr^{3+} sites [10,18,19]. Morterra et al. have shown that CO adsorbed onto Zr^{4+} sites is marked by a two-band complex at 2191 and 2186 cm^{-1}. CO adsorbed onto Zr^{3+} sites results in absorption bands at lower wavenumbers, near 2125 and 2112 cm^{-1} [19].

The infrared spectra of CO adsorbed on a ZrO_2 sample in the presence of 68 Torr of CO as a function of ZrO_2 activation temperature are shown in figure 2. Gas-phase contributions to the spectra shown in figure 2 have been subtracted out. The bands at 2191 and 2186 cm^{-1} are associated with the complex formed from CO adsorbed on Zr^{4+} sites, in agreement with the earlier results of Morterra et al. [19]. At lower wavenumbers, two bands are resolved at 2122 and 2101 cm^{-1}. The 2122 cm^{-1} band is in close agreement with frequencies previously reported, however, the 2101 cm^{-1} band is lower than previously reported values. The difference in frequencies of the bands observed in this study and previous studies may be due to the differences in the phases present in the samples. The samples used in this study contain ZrO_2 in both the monoclinic and tetragonal phases while the samples used in the study by Morterra et al. were 95% monoclinic. As the 2122 cm^{-1} band agrees with previous results of CO adsorbed onto Zr^{3+} sites, this is assigned to Zr^{3+} sites of the monoclinic phase and the 2101 cm^{-1} band is assigned to CO adsorbed on Zr^{3+} sites of the tetragonal phase.

Figure 3 shows a plot of the ratio of the integrated areas of CO coordinated to Zr^{3+} sites to CO coordinated to Zr^{4+} sites as a function of sample activation temperature. The plot in figure 3 shows that, at sample activation temperatures between 500 and 550°C, the ratio of the integrated areas of the bands associated with the Zr^{3+}–CO and Zr^{4+}–CO complexes remains nearly constant. As the sample activation temperature is increased above 550°C, there is an increase in the integrated area of the band associated with the Zr^{3+}–CO complex relative to the Zr^{4+}–CO complex. The increase in the integrated area of the Zr^{3+}–CO complex absorption band is associated with an increase in the number of Zr^{3+} sites accessible at the surface relative to the Zr^{4+} sites. It should be noted that both the Zr^{3+} and Zr^{4+} site coverage increase with temperature, from 500 to 600°C, although the Zr^{3+} site coverage increases more at 600°C, as shown in figure 3. At sample activation temperatures above 600°C, the Zr^{3+} site coverage continues to increase while the Zr^{4+} site coverage begins to decrease and the ratio of Zr^{3+} : Zr^{4+} surface sites increases sharply. This is similar to what is observed for other metal oxides; that is the defect site density increases with activation temperature as the sample becomes reduced [7,8]. The importance of both Zr^{4+}

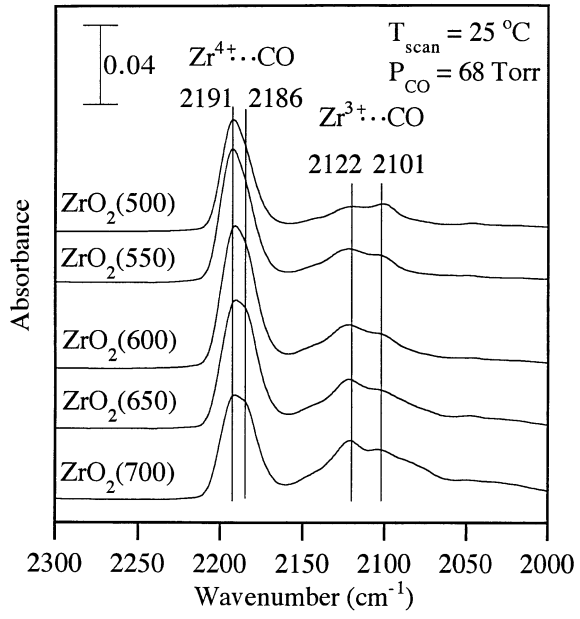

Figure 2. Transmission infrared spectra recorded of CO adsorbed on ZrO_2 activated at different temperatures between 500 and 700°C, at an equilibrium CO pressure of 68 Torr. Gas-phase contributions to the spectra have been subtracted out.

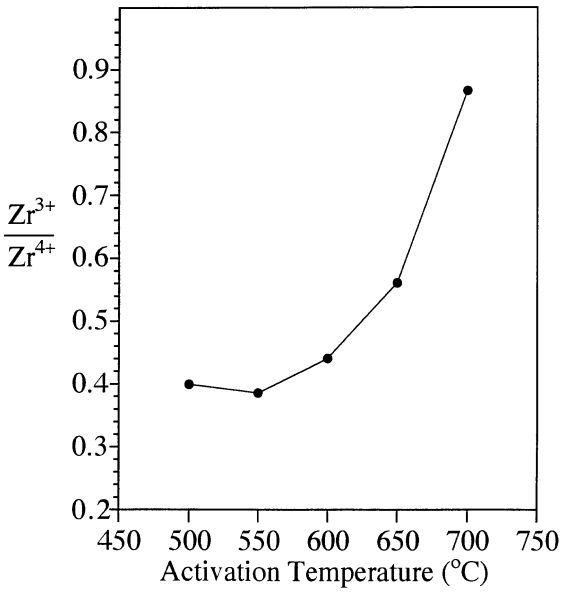

Figure 3. A plot of the ratio of the integrated areas of the absorption band of the Zr^{3+} ··· CO complex to the Zr^{4+} ··· CO complex as a function of ZrO_2 activation temperatures. The plot shows that the Zr^{3+} site coverage increases relative to the Zr^{4+} site coverage as the sample activation temperature increases.

and Zr^{3+} sites for N_2O adsorption and decomposition is discussed below.

3.2. Room temperature adsorption of N_2O on ZrO_2 activated at different temperatures

The IR spectra of N_2O, $^{14}N_2O$ and $^{15}N_2O$, adsorbed at room temperature on ZrO_2 activated near 500°C in the presence of 20 Torr of N_2O is shown in figure 4. Gas-phase contributions have been subtracted from the spectra. For adsorbed $^{14}N_2O$, the spectrum is characterized by two intense bands at 2242 and 1237 cm^{-1} assigned to the asymmetric (ν_{as}) and symmetric (ν_s) stretching modes, respectively, [3] of adsorbed $^{14}N_2O$. These two bands, ν_{as} and ν_s, shift by approximately +18 and −45 cm^{-1}, respectively, from the gas-phase values. In an earlier study [3], we have shown that the shift in frequencies of these vibrational modes is characteristic of N_2O bonded to the zirconia surface through the oxygen atom. Through the use of site-blocking molecules, it was shown, that N_2O molecularly adsorbs on Zr^{4+} sites. For adsorbed $^{15}N_2O$, the spectrum is characterized by two intense bands at 2171 (ν_{as}) and 1221 (ν_s) cm^{-1}. These bands undergo a frequency shift by −71 and −16 cm^{-1}, respectively, from adsorbed $^{14}N_2O$, as expected. Upon evacuation of gas-phase N_2O, absorption bands due to molecularly adsorbed N_2O disappear from the spectrum, indicating that molecular adsorption of N_2O on Zr^{4+} sites is reversible.

As shown previously [3], there is an increase in the integrated area of the ν_{as} and ν_s absorption bands of adsorbed N_2O for samples activated at 700°C compared to 450°C. This is consistent with an increase in the surface coverage of Zr^{4+} sites as the surface is dehydroxylated. Interestingly, there are no new absorption bands present in the spectrum that can be associated with N_2O coordinated to Zr^{3+} sites. However, as discussed below, there is evidence for N_2O decomposition at these reduced sites.

Although there is no catalytic decomposition of N_2O on ZrO_2 at room temperature, there is the possibility that N_2O dissociates on the ZrO_2 surface at this temperature to some limited extent. In order to determine if N_2O dissociates on ZrO_2 at room temperature, CO adsorption was used as a probe to determine if the coverage of surface defect sites, Zr^{3+} sites in particular, change upon N_2O adsorption. If N_2O decomposed on Zr^{3+} sites via the extraction of the oxygen atom in N_2O, then the coverage of these sites should decrease after reaction. The spectra recorded of adsorbed CO before and after room temperature adsorption of N_2O on ZrO_2(650) are shown in figure 5. The integrated area of the absorption band due to the Zr^{3+}–CO complex decreases by 23% from its initial value after N_2O adsorption. The integrated area of the Zr^{4+}–CO complex remains approximately constant before and after N_2O adsorption. The CO adsorption data suggest that N_2O decomposes on Zr^{3+} sites at temperatures as low as 25°C.

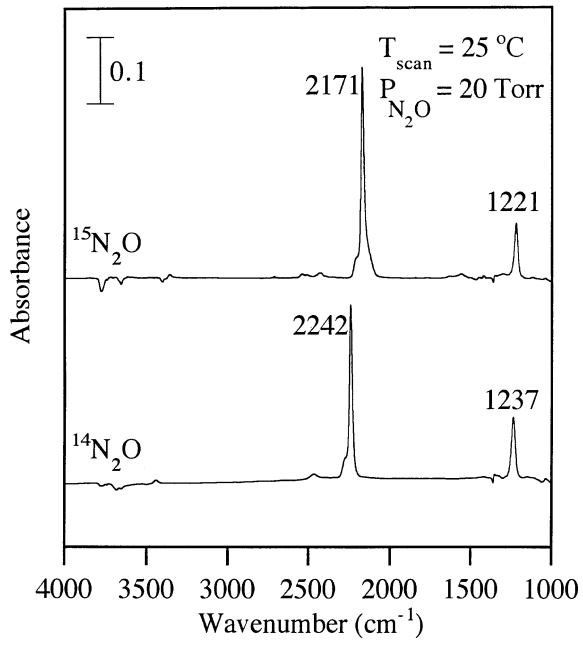

Figure 4. Transmission infrared spectra of $^{14}N_2O$ and $^{15}N_2O$ adsorbed on ZrO_2(500) in the presence of an equilibrium pressure, approximately 20 Torr, of gas-phase nitrous oxide. Gas-phase contributions to the spectra have been subtracted out.

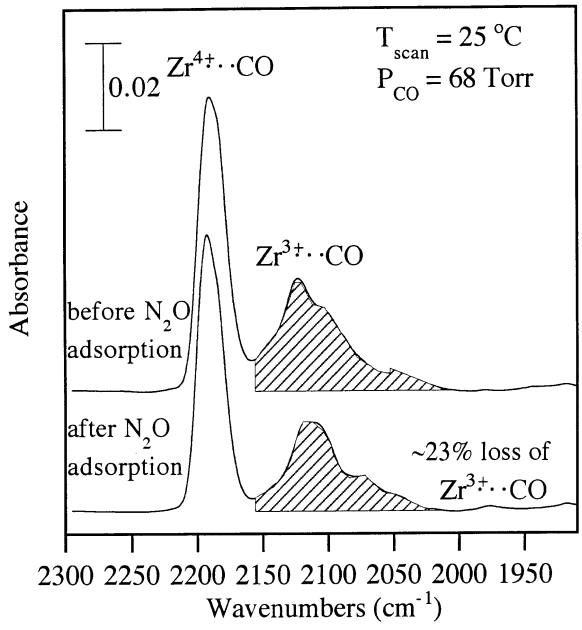

Figure 5. CO adsorbed on ZrO_2(650) before N_2O was adsorbed, top spectrum, and after N_2O was adsorbed and evacuated, bottom spectrum. Gas-phase contributions have been subtracted from the adsorbed spectra. There is a 23% loss in area of the absorption bands due to the $Zr^{3+}\cdots CO$ complex after N_2O adsorption.

3.3. N_2O decomposition on ZrO_2 at temperatures above 350°C

The N_2O decomposition reaction at higher temperatures was monitored with both IR spectroscopy and mass spectrometry. As discussed previously [3], catalytic decomposition of N_2O on ZrO_2 occurs at temperatures above 350°C. N_2O (70 Torr) was introduced into the sample cell that contained ZrO_2(500) and the gases from the reaction cell were leaked into the QMS chamber so that a RGA scan could be recorded. Another RGA scan was taken of the gas phase after reaction of N_2O on ZrO_2 for 1 h at 500°C. Under these conditions, approximately 60% of the N_2O reacted. Figure 6a shows a "difference" RGA scan, i.e. the RGA scan recorded after reaction for 1 h minus that from before reaction. Positive features, lines going up, at $m/e = 28$ and 32 are due to formation of molecular nitrogen and oxygen, respectively, as the reaction proceeds. Negative features, lines going down, at $m/e = 46$ and 30 are due to the decrease in pressure of N_2O as the reaction proceeds. The $m/e = 46$ ion is associated with the parent, N_2O^+, and $m/e = 30$ is associated with NO^+, a mass fragment of N_2O.

The N_2O decomposition reaction between 400 and 600°C showed that, similar to other studies on metal oxides, N_2O decomposition over ZrO_2 follows first-order reaction kinetics in N_2O pressure [20–23]. The kinetics of the decomposition reaction were monitored with IR spectroscopy. Infrared spectra were recorded of the gas phase at 10 min intervals, the initial pressure of N_2O was 100 Torr. The integrated areas of both gas-phase absorption bands were measured as the reaction proceeded. The data obtained at 500°C are plotted in figure 7. The rate constant is determined to be 0.24 ± 0.03 min^{-1} per gram of catalyst at 500°C. The error in the measurement represents one standard deviation in the values obtained for five different runs. The kinetics were not affected very much by catalyst activation temperature for samples activated between 500 and 700°C. However, the Zr^{3+} site coverage decreased significantly after the decomposition reaction, as measured by post-reaction CO adsorption.

In order to definitively determine whether N–O bond breakage exclusively occurred during N_2O decomposition, $^{14}N_2O$ and $^{15}N_2O$ were reacted over ZrO_2(500) at 500°C. 1.2 Torr each of $^{14}N_2O$ and $^{15}N_2O$ was introduced to the sample cell connected to the QMS chamber. The reactant gas was leaked into the QMS chamber and a RGA scan from $m/e = 1$–50 of the gas was taken. The leak valve was closed and the ZrO_2 catalyst was then heated to 500°C for 1 h and allowed to cool back to room temperature before a second RGA scan after reaction was taken. A resultant difference RGA scan is shown in figure 6b. Negative features at $m/e = 44$, 45, and 46, corresponding to $^{14}N_2O$, $^{14}N^{15}NO$, and $^{15}N_2O$, respectively, correlate with a decrease in the pressure of nitrous oxide after decomposition. The small amount of

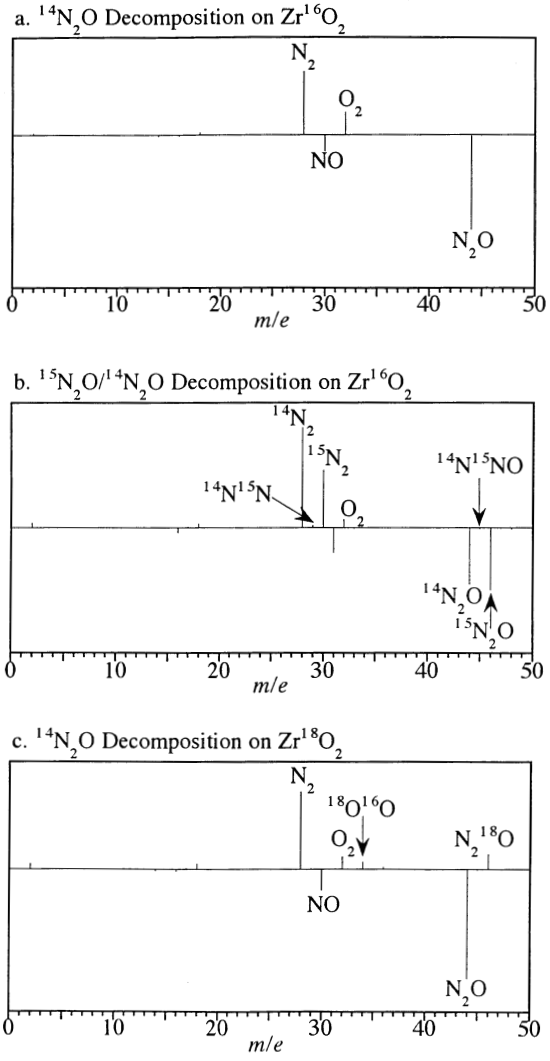

Figure 6. Difference RGA scan after the catalytic decomposition of N_2O on ZrO_2. Scans are shown for several isotope experiments. The positive features in the scan correspond to gases produced during reaction and the negative features in the scan correspond to gases that had reacted. (a) Difference RGA scan after N_2O decomposition at 500°C on ZrO_2(600). (b) Difference RGA scan after decomposition of a mixture of $^{14}N_2O/^{15}N_2O$ for 1 h at 500°C over ZrO_2(500). There is no evidence for isotopic scrambling to produce $^{14}N^{15}N$. The very small amount of $^{14}N^{15}N$ formed in the reaction is due to the decomposition of the $^{14}N^{15}NO$ impurity in the $^{15}N_2O$ sample. (c) Difference RGA scan after $N_2{}^{16}O$ decomposition at 500°C on ^{18}O-labeled $Zr^{18}O_2$(600).

$^{14}N^{15}NO$ initially present in the reaction cell corresponds to an impurity in the $^{15}N_2O$ gas. Positive features are seen at $m/e = 28$, 29, 30 and 32, corresponding to $^{14}N_2$, $^{14}N^{15}N$, $^{15}N_2$ and $^{16}O_2$, respectively. Although the initial pressures of $^{14}N_2O$ and $^{15}N_2O$ are nearly the same, the $^{15}N_2$ peak appears to be smaller than the $^{14}N_2$ peak. This is because $m/e = 30$ corresponds to two species $^{15}N_2$ and ^{14}NO. ^{14}NO is mass fragment of $^{14}N_2O$. Therefore, the peak has two contributions, $^{15}N_2$, which is increasing during decomposition, and ^{14}NO, which is decreasing during decomposition. The negative feature

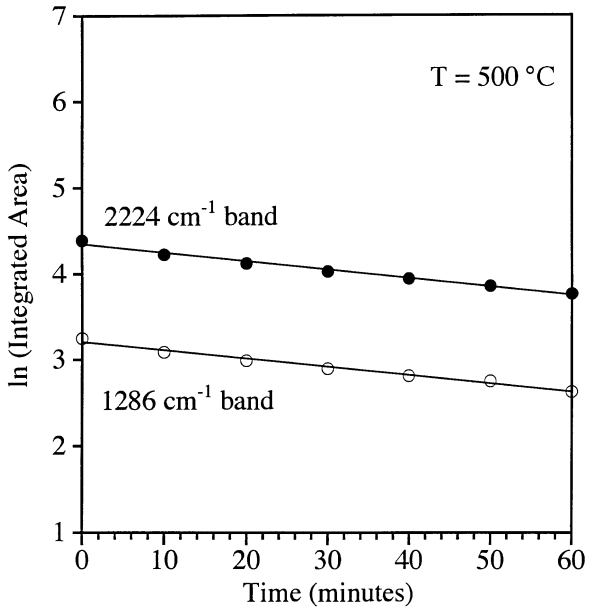

Figure 7. Kinetic data for N_2O decomposition on $ZrO_2(600)$ at 500°C. As shown in the plot above, the loss of N_2O follows first-order reaction kinetics.

at $m/e = 31$ corresponds to ^{15}NO, a mass fragment of $^{15}N_2O$.

If complete isotopic scrambling was to occur, it would be expected that the ratio of the intensity of the three molecular nitrogen ions $^{14}N^{14}N : {}^{14}N^{15}N : {}^{15}N^{15}N$ ($m/e = 28 : 29 : 30$) after decomposition would be 1 : 2 : 1 after taking into account mass fragmentation. However, if there was no isotopic scrambling, there would only be a very small positive feature at $m/e = 29$ due to the small amount of $^{14}N^{15}N$ that decomposed formed from the decomposition of the $^{14}N^{15}NO$ impurity. As clearly observed in the difference RGA scan shown in figure 6b, there is only a small amount of $^{14}N^{15}N$ produced relative to the amounts of $^{14}N_2$ and $^{15}N_2$. The small $^{14}N^{15}N$ signal can be attributed to the decomposition of $^{14}N^{15}NO$ impurity in the $^{15}N_2O$ labeled gas. From this experiment, it is concluded that isotopic scrambling does not occur and the N–N bond remains intact during the decomposition reaction.

3.4. ^{18}O exchange between $C^{18}O_2$ and ZrO_2

Additional mechanistic studies were done to determine if lattice oxygen atoms became incorporated into product O_2 molecules. ^{18}O labeling of either N_2O or ZrO_2 would address this issue. It was determined that ^{18}O labeling of the ZrO_2 catalyst was the most practical method. ^{18}O incorporation into ZrO_2 was accomplished with $C^{18}O_2$ in a procedure adapted from that used by Yanagisawa et al. for exchange of oxygen with MgO [24].

Initially, 60 Torr $C^{18}O_2$ was introduced to $ZrO_2(600)$ at room temperature and then heated to 600°C for 1 h. Figure 8 shows a difference residual gas analysis before and after heating. As can be seen, there is a decrease in the amount of $C^{18}O_2$, while there is an increase in the amount of $C^{16}O^{18}O$. The mass spectral data show that there is single exchange of oxygen under these conditions and that ^{18}O atoms are incorporated into the ZrO_2 sample. Further experiments have shown that at this reaction temperature, the exchange reaction has proceeded to its fullest extent after just 3 min of reaction.

The amount of ^{18}O incorporation into the ZrO_2 catalyst was calculated as follows. First, the number of ^{18}O atoms exchanged between gaseous carbon dioxide and the surface was determined. It was found that approximately 20% of the $C^{18}O_2$ reacted. The number of $C^{18}O_2$ molecules reacted was determined to be near 2×10^{20} and because a single exchange takes place, this corresponds to the number of ^{18}O atoms incorporated into the zirconia catalyst. Next, the surface density of oxygen atoms was estimated from the bulk density of ZrO_2 [25], assuming a surface depth of 2 Å. In these calculations, the average of the densities for the monoclinic and tetragonal phases was used. The surface coverage of oxygen atoms is established to be 1.1×10^{15} cm^{-2}.

The surface area of the ZrO_2 nanoparticle powders used in this study is 78 m^2/g. For the exchange experiment, 0.0234 g of ZrO_2 were pressed into the grid, giving a total surface area of 1.8 m^2. Therefore, there are approximately 2×10^{19} surface oxygen atoms. Given that 2×10^{20} ^{18}O reacted (vide supra), it is concluded that approximately ten layers underwent exchange. This

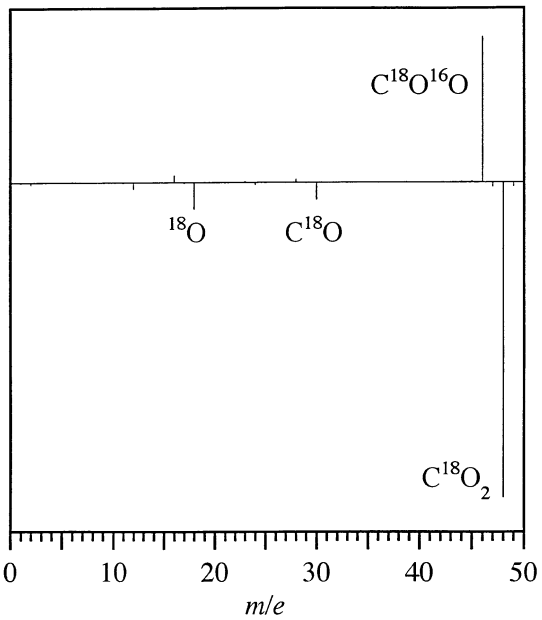

Figure 8. Difference RGA scan after heating $C^{18}O_2$ at 600°C for 1 h in the presence of $ZrO_2(600)$. As in figure 6, the positive features in the scan correspond to gases produced during reaction, $C^{18}O^{16}O$, and the negative features correspond to gases that had reacted.

is admittedly a rough calculation, but it does show that ^{18}O atoms have been incorporated into the zirconia catalyst at the surface and in the near-surface region.

3.5. N_2O decomposition on $Zr^{18}O_2$

After the sample had been ^{18}O labeled, the N_2O decomposition reaction was done at 500°C for 1 h. Figure 6c shows the difference RGA scan before and after decomposition. For the labeled catalyst, besides N_2 and $^{16}O_2$ formation, there is also $^{18}O^{16}O$ and a small amount of $^{18}O_2$. Neither $^{18}O^{16}O$ nor $^{18}O_2$ are formed in the absence of N_2O. These results indicate that lattice oxygen atoms become incorporated into product O_2 molecules during decomposition.

There is also some formation of $N_2{}^{18}O$ ($m/e = 46$) that corresponds to a product of the back reaction between N_2 and adsorbed oxygen atoms. This raises the question of whether the ^{18}O in the products is the sole result of decomposition of this back reaction. In a separate experiment, the rates of formation of $N_2{}^{18}O$ and $^{16}O^{18}O$ were monitored. It was found that the rate of formation of $^{16}O^{18}O$ decreased before the amount of $N_2{}^{18}O$ reached its peak. If $^{16}O^{18}O$ was formed only from the reaction of $N_2{}^{18}O$, the rate of its formation would be a maximum when the amount of $N_2{}^{18}O$ was a maximum. Therefore, this indicates that there is another source of ^{18}O for $^{16}O^{18}O$ besides the decomposition of $N_2{}^{18}O$ and that this source is depleted before the amount of $N_2{}^{18}O$ has reached its highest value. The only other source of ^{18}O would be from the labeled ZrO_2 catalyst. The evidence shows there is direct incorporation of lattice oxygen atoms into product oxygen molecules.

4. Discussion

4.1. Molecular and dissociative adsorption of ZrO_2 at room temperature

It was shown here that as the catalyst activation temperature increases, the surface becomes dehydroxylated and oxygen deficient. The defect site density, i.e. the coverage of Zr^{3+} sites increases by a factor of two as the activation temperature is raised from 500 to 700°C. Previously we had shown that N_2O molecularly adsorbs on Zr^{4+} sites at room temperature in the presence of gas-phase N_2O [3]. Results from this study show that not only does N_2O molecularly adsorb on ZrO_2 at room temperature but there is some decomposition as well. The decomposition of N_2O is evident by a decrease in the amount of Zr^{3+} sites after N_2O adsorption, as determined by a decrease in the adsorption capacity for CO on these sites. The amount of decomposition is small as there is no significant loss of gaseous N_2O or any significant formation of N_2 or O_2 at room temperature. These results suggest that a limited amount of N_2O decomposes at room temperature and the oxygen atom extracted from the N_2O molecule on Zr^{3+} sites remains on the surface at $T = 25$°C. The decomposition of N_2O on ZrO_2 at low temperatures, between 183 and 303 K, was also recently observed by Aika and Iwamatsu [26].

4.2. Active sites for N_2O decomposition on ZrO_2 above 350°C

At temperatures above 350°C, N_2O undergoes catalytic decomposition on ZrO_2 to yield N_2 and O_2 exclusively. CO adsorption in conjunction with IR spectroscopy, showed that the Zr^{3+} site coverage decreased significantly after reaction of N_2O at temperatures above 350°C. The data suggest that Zr^{3+} sites are active sites for N_2O decomposition at high temperatures as well as at low temperatures.

4.3. Role of lattice oxygen atoms in N_2O decomposition on ZrO_2

The role of lattice oxygen atoms in metal oxide catalyzed reactions is typically investigated through the use of ^{18}O labeling experiments. Using $H_2{}^{18}O$ as the precursor, Li and Klabunde found for MgO with a surface area of 130 m^2/g, 1.9 layers were exchanged at a reaction temperature of 500°C and 9.3 layers at a temperature of 700°C [27]. For MgO with a surface area of 390 m^2/g, 1.5 layers were exchanged at 500°C and 7.9 layers at 700°C. It was found that at temperatures below 500°C, exchange occurred only at the surface. This is consistent with previously reported results of isotope exchange between ionic solids and diatomic gases [28–30].

In a study by Yanagisawa et al. using $C^{18}O_2$ to label the oxygen atoms in MgO, it was found that both single and double exchange of oxygen atoms occurred with $C^{18}O_2$, depending upon the temperature at which the reaction was done, with double exchange favored at the higher temperatures studied [24]. In this study, $C^{18}O_2$ was chosen as the labeling reagent because it could potentially undergo double exchange with the lattice oxygen atoms of ZrO_2. However, the mass spectral data clearly show that single exchange preferentially took place at 600°C. In addition, our calculations indicate that exchange is not limited to the surface, but that ^{18}O may migrate into the lattice a few layers. The possible participation of lattice oxygen atoms in the nitrous oxide decomposition reaction was then studied by reaction of N_2O on $Zr^{18}O_2$. The incorporation of ^{18}O from the $Zr^{18}O_2$ catalyst into product oxygen molecules is observed, as the mass spectral data clearly show the production of $^{18}O^{16}O$. This mass spectral/isotope experiment establishes that lattice oxygen atoms become incorporated into product oxygen molecules and must be included as a step in the detailed reaction mechanism of N_2O decomposition on ZrO_2 as discussed below.

4.4. Reaction mechanism for N_2O decomposition on ZrO_2

The mixed labeled nitrogen experiment, $^{14}N_2O/^{15}N_2O$ (figure 6b), shed additional light on the reaction mechanism of nitrous oxide decomposition on zirconia. The experiment showed that isotopic scrambling of $^{14}N_2O$ and $^{15}N_2O$ to form $^{14}N^{15}N$ does not occur. This is an important result for two reasons. First, it clearly establishes that the nitrogen–oxygen bond exclusively breaks in the decomposition reaction. Second, as discussed in section 1, there is some interest in recycling N_2O produced in adipic acid synthesis back to the nitric acid feed. The results presented here show that zirconia would not be a good catalyst for the conversion of nitrous oxide to nitric acid as the N–N bond remains intact.

The second isotope experiment, using the ^{18}O-labeled catalyst, showed that surface lattice oxygen atoms in ZrO_2 do participate in the reaction and are incorporated into the molecular oxygen product from the direct reaction of $N_2{}^{16}O$ on $Zr^{18}O_2$. Additional experiments were done to monitor the amount of $^{16}O^{18}O$ formed during reaction as a function of time (not shown). It was found that the $^{16}O^{18}O$ pressure increased very quickly during the first few minutes of reaction, at a rate nearly equal to that of the growth of the amount of $^{16}O^{16}O$. After about 5 min at 500°C, however, the growth in the amount of $^{16}O^{18}O$ slowed considerably as the ^{18}O in the lattice become depleted. Within 15 min after reaction started, the growth in the amount of $^{16}O^{18}O$ is very slow. The growth at longer times may be due to the decomposition of $N_2{}^{18}O$. ($N_2{}^{18}O$ is formed from the back reaction of $N_2 + {}^{18}O$.)

Taking all of the results presented here, the mechanism for N_2O decomposition on ZrO_2 can be deduced. First, N_2O dissociates on the surface at defect sites, i.e. Zr^{3+} sites, leaving oxygen atoms adsorbed on the surface. The decomposition reaction most likely proceeds through an electron transfer reaction at the reduced Zr^{3+} site to form N_2O^- as a transient intermediate, as has been previously postulated for N_2O decomposition [20–23,31]:

$$N_2O(a) \rightarrow [N_2O^-(a)] \rightarrow N_2(g) + O(a), \quad \text{at } Zr^{3+} \text{ sites}. \tag{1}$$

Adsorbed O atoms from N_2O decomposition, O(a), can react with either lattice oxygen atoms, O(L), or another adsorbed oxygen:

$$O(a) + O(L) \rightarrow O_2(g) \tag{2}$$

$$O(a) + O(a) \rightarrow O_2(g) \tag{3}$$

Evidence for the reaction shown in eq. (3) can be found by monitoring the production of $^{16}O^{16}O$ during reaction over the labeled catalyst. As discussed above, the signal intensities of the mass spectrometer signal for $^{16}O^{16}O$ and $^{16}O^{18}O$ initially grow at nearly the same rate. Since the lattice oxygen atoms at the surface of the catalyst are ^{18}O labeled, the probability of an ^{16}O from N_2O reaction with an ^{16}O lattice oxygen is minimal. Therefore, the combination of two adsorbed oxygen atoms from nitrous oxide decomposition is the only source of ^{16}O, as shown in eq. (3). It is important to note that $^{16}O^{18}O$ and $^{16}O^{16}O$ are produced at approximately the same rates in the initial stages of the reaction indicating that steps (2) and (3) proceed at nearly the same rate. The ability of ZrO_2 to provide an additional source of oxygen atoms to form molecular oxygen may be the reason that ZrO_2 is found to be such a good catalyst for nitrous oxide decomposition.

Several rate expressions have been derived for N_2O decomposition on metal oxides [20–23]. These rate expressions are:

$$\text{rate} = kP(N_2O), \tag{4}$$

$$\text{rate} = kP(N_2O)[1 + bP(O_2)^{-1/2}]^{-1}, \tag{5}$$

$$\text{rate} = kP(N_2O)P(O_2)^{-1/2}. \tag{6}$$

For all of these rate expressions, the rate is first order in N_2O pressure. The rate expression shown in eq. (4) applies when N_2O adsorption is rate-limiting and there is no dependence on oxygen pressure. The rate expressions shown in eqs. (5) and (6) apply to N_2O decomposition mechanisms that are rate-limited to some extent by oxygen desorption and therefore, the rate expression has an oxygen pressure dependence. The rate expressions given in eqs. (5) and (6) are for two limiting cases of weak and strong inhibition of molecular oxygen on the reaction rate, respectively. A full kinetic analysis of the rate data has not been attempted here. Therefore, the rate expression for N_2O decomposition may perhaps not follow the simple reaction rate law given in eq. (4) but may indeed have an oxygen pressure dependence.

5. Conclusions

In this study, nitrous oxide adsorption and decomposition on ZrO_2 were investigated. Several conclusions can be drawn from the studies presented here. First, at temperatures below any catalytic decomposition of N_2O, there is evidence for both molecular and dissociative adsorption on ZrO_2. At 25°C, N_2O molecularly adsorbs through the oxygen end of the molecule on Zr^{4+} sites and dissociative adsorption of N_2O occurs on surface defect sites, i.e. Zr^{3+} sites. Second, at higher temperatures Zr^{3+} sites are active toward N_2O dissociation as well. Above 350°C, the catalytic decomposition of N_2O on ZrO_2 follows first-order reaction kinetics with respect to N_2O pressure. Third, isotopes studies in con-

junction with mass spectrometry provided further insight into N_2O decomposition on ZrO_2. In particular, evidence was presented to show that N–N bond dissociation did not occur and that lattice oxygen atoms become incorporated into product oxygen molecules during the reaction.

Acknowledgement

The authors would like to gratefully acknowledge support from the National Science Foundation (CHE-9614134) and du Pont de Nemours and Co. The authors would also like to thank Drs. Sau Lan Tang and Theodore A. Koch (at du Pont) for helpful discussions during the course of this work.

References

[1] M.H. Theimens and W.C. Trogler, Science 251 (1991) 932.
[2] R. Reimer, C.S. Slaten, M. Seapan, M.W. Lower and P.E. Tomlinson, Environm. Progr. 13 (1994) 134.
[3] T.M. Miller and V.H. Grassian, J. Am. Chem. Soc. 117 (1995) 10969.
[4] K. Anseth and T.A. Koch, US Patent 5314673.
[5] H.C. Zeng, J. Lin, W.K. Teo, J.C. Wu and K.L. Tan, J. Mater. Res. 10 (1995) 545.
[6] V.E. Henrich and P.A. Cox, *The Surface Science of Metal Oxides* (Cambridge University Press, Cambridge, 1994).
[7] M.A. Barteau, J. Vac. Soc. Technol. A 11 (1993) 2162.
[8] A.A. Davydov, *Infrared Spectroscopy of Adsorbed Species on the Surface of Transition Metal Oxides*, ed. C.H. Rochester (Wiley, New York, 1990).
[9] C. Morterra, E. Giamello, L. Orio and M. Volante, J. Phys. Chem. 94 (1990) 3111.
[10] Z.X. Liu, Q.X. Bao and N.J. Wu, J. Catal. 113 (1988) 45.
[11] J. Haber and E.M. Serwicka, React. Kinet. Catal. Lett. 35 (1987) 369.
[12] J.B. Black, J.D. Scott, E.M. Serwicka and J.B. Goodenough, J. Catal. 106 (1987) 16.
[13] Z.X. Liu, K. Xie, Y.Q. Li and Q.X. Bao, J. Catal. 119 (1989) 249.
[14] M.E. Lashier and G.L. Schrader, J. Catal. 128 (1991) 113.
[15] T. Jin, T. Okuhara, G.J. Mainsand and J.M. White, J. Phys. Chem. 91 (1987) 3310.
[16] P. Basu, T.H. Ballinger and J.T. Yates Jr., Rev. Sci. Instrum. 59 (1988) 1321.
[17] T. Yamaguchi, Catal. Today 20 (1994) 199.
[18] K.-H. Jacob, E. Knozinger and S. Benfer, J. Chem. Soc. Faraday Trans. 90 (1994) 2969.
[19] C. Morterra, L. Orio and C. Emanuel, J. Chem. Soc. Faraday Trans. 86 (1990) 3003.
[20] (a) E.R.S. Winter, J. Catal. 15 (1969) 144;
(b) E.R.S. Winter, J. Catal. 34 (1974) 431.
[21] S.L. Raj, B. Viswanathan, and V. Srinivasan, Ind. J. Chem. 21A (1982) 689.
[22] J.F. Read, J. Catal. 28 (1973) 428.
[23] A. Cimino, V. Indova, F. Pepe and F.S. Stone, Gaz. Chim. Ital. 103 (1973) 935.
[24] Y. Yanagisawa, K. Takaoka and S. Yamabe, J. Chem. Soc. Faraday Trans. 90 (1994) 2561.
[25] R. Stevens, *Zirconia and Zirconia Ceramics* (Magnesium Elektron, 1986).
[26] K. Aika and E. Iwamatsu, in: *Studies in Surface Science and Catalysis*, Vol. 90, eds. H. Hattori, M. Misono and Y. Ono (Elsevier, Amsterdam, 1994).
[27] Y.-X. Li and K. Klabunde, Chem. Mater. 4 (1992) 611.
[28] G.K. Boreskov, Adv. Catal. 15 (1964) 285.
[29] G.K. Boreskov, Discuss. Faraday Soc. 41 (1966) 263.
[30] L.G. Harrison and J.A. Morrison, J. Phys. Chem. 62 (1958) 372.
[31] Z. Sojka and M. Che, J. Phys. Chem. 100 (1996) 4776.